

Vision-based Deck State Estimation for Autonomous Ship-board Landing

Benjamin L. Truskin

blt5050@psu.edu

Graduate Research Assistant

The Pennsylvania State University, Aerospace Department

University Park, PA, U.S.A

Jack W. Langelaan, Ph. D.

jlangelaan@psu.edu

Associate Professor of Aerospace Engineering

The Pennsylvania State University, Aerospace Department

University Park, PA, U.S.A

ABSTRACT

This paper describes a method for ship deck estimation using only sensing carried aboard an autonomous rotorcraft: specifically, sensing is limited to a vision system, an inertial measurement unit and GPS. Using bearings to features on the ship deck and knowledge of helicopter state provided by the INS/GPS, a state estimator computes estimates of deck state and covariance. This deck state estimate can then be used to compute a safe, feasible trajectory to landing. This paper presents an Unscented Kalman Filter based implementation that uses a generic second order kinematic model driven by zero mean Gaussian noise for the ship deck motion model: while this deck motion model contains significant unmodeled dynamics it is not specific to a particular ship. Results of Monte Carlo simulations illustrate the utility of the proposed approach: good estimation results are obtained for stochastic deck motion (with a Pierson-Moskowitz power spectral density) and a fast ferry ship model.

INTRODUCTION

The use of autonomous vehicles is having a significant operational impact in both the commercial and military sectors. However, significant research challenges still remain.

Operations at sea adds a significant level of difficulty to launch and recovery operations. Not only are the aircraft subject to environmental disturbance, but the landing deck is now under the influence of currents and tides as well as the semi-random motion of waves. In order to safely attempt a landing, deck state must be estimated to a high degree of accuracy. In the case of non-specialized ships, where there is no specialized equipment on board and little to no communication between the ship and the helicopter, all sensors, computational ability, and controlling equipment must be kept onboard the aircraft.

While there is current capability for autonomous take-off and landing on ships, there are many restrictions. Northrop Grumman's MQ-8B Fire Scout UAV has been used in an operational environment, but take-off and landing has generally been restricted to fairly calm conditions and the use of a specially equipped ship. The Landing Period Designator (Ref. 1)

predicts when deck motion will be small so that a safe landing can be attempted by manned rotorcraft, but application to unmanned rotorcraft will still require an autonomous landing system. Tether-based landing systems (Ref. 2), while they can be effective, require specially equipped ships.

There has been extensive research in the use of vision systems for autonomous navigation and obstacle avoidance (Refs. 3–7), relative navigation and landing (Refs. 8–11) and landing on targets undergoing simple motion (Refs. 12, 13). Landing on a ship deck is significantly more complex, and systems involving fused vision, LIDAR, and GPS/INS have been proposed (Ref. 14).

The purpose of the research described in this paper is development of a system to enable autonomous take-off and landing from a ship deck in conditions exceeding sea state 5. Further, to ensure that the system can be used across a wide variety of vehicles operating from a wide variety of ships, sensing will be limited to only those devices that can be carried aboard the helicopter, and communications between ship and aircraft will be limited to a single message defining ship nominal heading and speed and current sea state. Specifically, sensing is limited to a monocular vision system, inertial measurement unit (IMU) and GPS. It is assumed that the IMU and GPS can provide helicopter state information and that the monocular vision system can provide bearing measurements to a set of features on the landing deck.

Presented at the AHS 69th Annual Forum, Phoenix, Arizona, May 21–23, 2013. Copyright © 2013 by the American Helicopter Society International, Inc. All rights reserved.

PROBLEM STATEMENT

Landing scenario

The scenario considered here consists of an autonomous helicopter landing on a moving ship deck (Figure 1). An on-board camera obtains measurements to features on the ship deck and a GPS/INS provides knowledge of helicopter state.

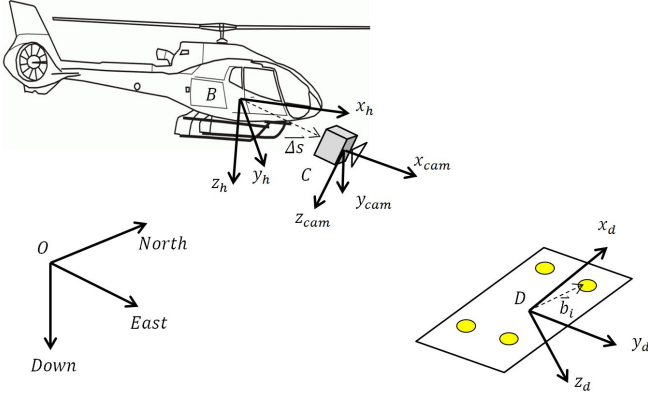


Fig. 1. A schematic depicting the estimation problem at hand.

The landing deck is undergoing unknown motion in frame O , an inertial north-east-down (NED) frame. Deck features are located at known positions \mathbf{b}_i in frame D , fixed to the deck. A transformation matrix \mathbf{T}_d resolves a vector in frame O to frame D . Sensors (i.e. the camera and GPS/INS) are fixed in the vehicle's body frame B . It is further assumed that the camera is located at a known stationary point in the body frame and that the orientation of the camera with respect to the body frame is known. Bearings to deck markers are obtained in the camera frame C . Transformation matrices \mathbf{T} and \mathbf{T}_{cam} define the transformation of a vector from O to B and from B to C , respectively.

The problem at hand is to estimate the state of the deck:

$$\mathbf{x}_d = [x_d \ y_d \ z_d \ \phi_d \ \theta_d \ \psi_d \ u_d \ v_d \ w_d \ p_d \ q_d \ r_d]^T \quad (1)$$

given knowledge of helicopter state

$$\mathbf{x}_h = [x_h \ y_h \ z_h \ \phi_h \ \theta_h \ \psi_h \ u_h \ v_h \ w_h]^T \quad (2)$$

and bearings to deck markers. Here x, y, z denote position in the inertial frame, ϕ, θ, ψ denote orientation with respect to the inertial frame, u, v, w denote velocities and p, q, r denote body-axis angular rates. In the case of the ship deck, velocities are expressed in the inertial frame O ; in the case of the helicopter, velocities are expressed in the vehicle body frame B .

This deck state information can then be used by a planning and control algorithm to compute (and fly) a safe path to landing on the deck.

There are two sources of nonlinearity in the deck state estimation problem. The most significant is in the measurements of bearing to deck markers: the vision system projects the three dimensional world onto the two dimensional image plane. Second is the nonlinearity of the deck's rotational motion. Because of the nonlinearity of the measurement model, the path flown during approach can have a significant impact on the accuracy of deck state estimation. However, planning this path to maximize knowledge gained is not the focus of this paper.

System description

The block diagram in Figure 2 shows a system that uses the given sensors to perform autonomous landing.

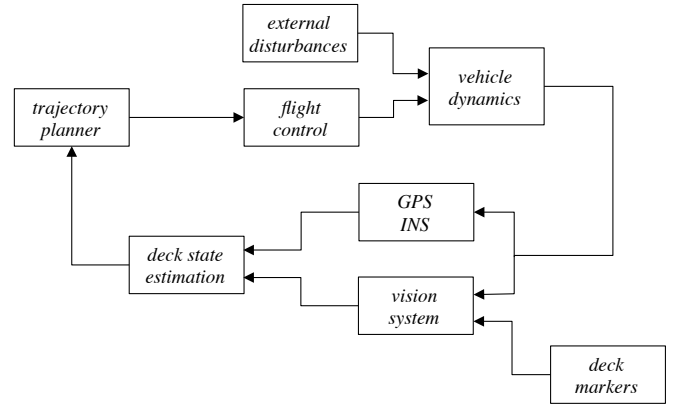


Fig. 2. Landing system top-level block diagram.

Helicopter state information is fused with bearings to deck markers to compute an estimate of ship deck state in an estimator. The trajectory planner uses the deck state estimate to compute a safe, feasible trajectory to landing, and a flight control system follows the trajectory.

Given the limited sensing available and the unknown wave states driving ship deck motion, the problem at hand is to obtain enough information about the deck state to permit a safe landing. That is, the problem is to compute an estimate $\hat{\mathbf{x}}_d$ and associated covariance \mathbf{P} of the deck state \mathbf{x}_d using a process model

$$\dot{\mathbf{x}}_d = f(\mathbf{x}_d, \mathbf{u}) \quad (3)$$

and measurement model

$$\mathbf{z} = g(\mathbf{x}_h, \mathbf{x}_d) \quad (4)$$

Here \mathbf{u} represents inputs and disturbances to the ship deck and \mathbf{z} represents measurements from the vision system sensors.

Sensor and system models

Deck Kinematic Model To keep the deck motion model general across a wide variety of ships and boats a second order

kinematic model driven by zero-mean Gaussian noise is used. This is a constant acceleration model (in fact, it assumes that average acceleration is zero), and clearly there will be significant unmodeled dynamics (acceleration of a ship deck driven by wave motion is not constant, although it is zero mean over a long enough time window). However, the ease of implementation and broad applicability of this model makes it an attractive choice.

Both deck position and velocity are expressed in the inertial frame, so that

$$\dot{x}_d = u_d \quad (5)$$

$$\dot{y}_d = v_d \quad (6)$$

$$\dot{z}_d = w_d \quad (7)$$

Body angular rates can be expressed as Euler angle rates by

$$\dot{\phi}_d = p_d + q_d \sin \phi_d \tan \theta_d + r_d \cos \phi_d \tan \theta_d \quad (8)$$

$$\dot{\theta}_d = q_d \cos \phi_d - r_d \sin \phi_d \quad (9)$$

$$\dot{\psi}_d = q_d \frac{\sin \phi_d}{\cos \theta_d} + r_d \frac{\cos \phi_d}{\cos \theta_d} \quad (10)$$

Deck acceleration and angular acceleration are driven by unknown forcing functions

$$\dot{u}_d = F_{du} \quad (11)$$

$$\dot{v}_d = F_{dv} \quad (12)$$

$$\dot{w}_d = F_{dw} \quad (13)$$

$$\dot{p}_d = F_{dp} \quad (14)$$

$$\dot{q}_d = F_{dq} \quad (15)$$

$$\dot{r}_d = F_{dr} \quad (16)$$

Ultimately, deck motion is forced by waves acting upon the ship. To avoid a specific ship model, here the forcing term

$$\mathbf{F}_d = [F_{du} \ F_{dv} \ F_{dw} \ F_{dp} \ F_{dq} \ F_{dr}]^T \quad (17)$$

is assumed be zero-mean Gaussian random noise:

$$\mathbf{F}_d \sim \mathcal{N}(0, \mathbf{Q}) \quad (18)$$

The covariance \mathbf{Q} of this forcing term must be large enough to “cover” the unmodeled dynamics. It will be determined based on sea state. The actual value of the covariance of \mathbf{Q} is described in a later section.

Vision Model The camera is located at a known position Δs from the helicopter center of gravity with a known rotation \mathbf{T}_{cam} with respect to the vehicle body frame. The camera’s x -axis is the optical axis, so that camera y and z axes lie in the image plane.

For a vector \mathbf{s} expressed in the camera frame, the pinhole projection model defines that vector’s projection onto the image plane:

$$\mathbf{z} = \frac{f}{s_x} \begin{bmatrix} s_y \\ s_z \end{bmatrix} \quad (19)$$

where f is the focal length and s_x , s_y , and s_z denote the components of the vector expressed in the camera frame.

The pinhole projection model becomes ill conditioned for vectors that are nearly perpendicular to the optical axis. A modified pinhole model computes bearings (azimuth and depression angle: here a positive angle is down with respect to the camera’s optical axis) as the arctangent of the pinhole projection. For the i^{th} deck marker the vision model g_i is

$$\mathbf{z}_i = \begin{bmatrix} \arctan \left(\frac{s_{i,y}}{s_{i,x}} \right) \\ \arctan \left(\frac{s_{i,z}}{s_{i,x}} \right) \end{bmatrix} + \mathbf{n}_c \quad (20)$$

The measurement is corrupted by zero-mean Gaussian random noise \mathbf{n}_c . The vector \mathbf{s}_i represents the vector to the i^{th} marker, expressed in the camera frame:

$$\mathbf{s}_i = \mathbf{T}_{cam} \left[\mathbf{T} \begin{bmatrix} x_i - x_h \\ y_i - y_h \\ z_i - z_h \end{bmatrix} - \Delta s \right] \quad (21)$$

where $\mathbf{x}_i = [x_i \ y_i \ z_i]^T$ is the position of the i^{th} marker in the inertial frame. The position of a deck marker in the inertial frame is dependent on the deck position, deck orientation and the position of the marker in the deck frame:

$$\mathbf{x}_i = \begin{bmatrix} x_d \\ y_d \\ z_d \end{bmatrix} + \mathbf{T}_d^{-1} \mathbf{b}_i \quad (22)$$

where \mathbf{b}_i is the location of the i^{th} marker in the deck frame (assumed known).

Modeling Ship Deck Motion

Ship deck motion can be very complex: in essence it is the dynamics of the ship driven by wave motion. Ship motion modeling is not the focus of this paper, (and the deck model used in the estimator does not assume a specific motion model) but a brief discussion is warranted to give confidence in the deck state estimation results.

The simplest model of deck motion is perhaps six degree of freedom rigid body motion with independent sinusoidal forcing in each degree of freedom, so that

$$F_{d(\cdot)}(t) = -A_{(\cdot)} \omega_{(\cdot)}^2 \sin(\omega_{(\cdot)} t + \phi_{(\cdot)}) \quad (23)$$

Here A is the wave amplitude, ω is the frequency, and ϕ is phase. (\cdot) denotes a particular degree of freedom (u , v , w , p , q , r).

Integrating this forcing term twice gives simple sinusoidal motion for each degree of freedom with amplitude A , frequency ω and phase ϕ . Note that amplitude, frequency, and phase can be specified independently for each degree of freedom.

While this motion may “look” realistic when viewed as an animation, it is still regular, highly periodic motion. It is useful for basic testing of estimator performance, but a more realistic model of deck motion will give more confidence in performance.

Stochastic Method While something like a sinusoidal wave gives motion that “looks” realistic, in practice that function gives very regular motion. True ship motion is far less regular, with significant changes in motion amplitude from one wave to the next.

To model this more complex motion a sum-of-sinusoids is used, so that (Ref. 15):

$$F_{d(\cdot)}(t) = \sum_{k=1}^N -A_{(\cdot),k} \omega_{(\cdot),k}^2 \sin(\omega_{(\cdot),k} t + \varphi_{(\cdot),k}) \quad (24)$$

Choosing random, uniformly distributed values of $\varphi_{(\cdot),k}$ will give a wave shape that appears random. The problem now is making an appropriate choice of amplitudes $A_{(\cdot),k}$ and frequencies $\omega_{(\cdot),k}$: these can be computed after a particular wave power spectrum has been defined.

The Pierson-Moskowitz spectrum (Ref. 16) is an empirically derived power spectrum that defines wave energy as a function of frequency for a fully developed sea. The power spectral density is

$$S_{PM}(\omega) = \frac{0.78}{\omega^5} \exp\left(\frac{-3.11}{\omega^4 h_{1/3}^2}\right) \quad (25)$$

Here $h_{1/3}$ is the mean wave height, which is defined based on sea state. The frequency for peak power density is

$$\omega_0 = 1.26 h_{1/3}^{-0.5} \quad (26)$$

Sea state is a numerical designation ranging from 0 (glassy calm) to 9 (wave heights exceed fourteen meters) that defines wave height. Table 1 gives parameters for sea states 1, 5, and 7; Figure 3 shows the Pierson-Moskowitz amplitude spectrum for those sea states.

Table 1. Sea state, mean wind speed and Pierson-Moskowitz parameters

Seastate	windspeed (kt)	$h_{1/3}$ (m)	ω_{nom} (rad/s)	$\omega_{min} - \omega_{max}$ (rad/s)
1	7	1	3.14	1.8 – 6.28
5	23	2.5	1.05	0.57 – 1.8
7	43	6.5	0.526	0.3 – 0.97

To represent a wave condition that has the Pierson-Moskowitz spectral density, amplitudes for a set of frequencies ω_k and associated bandwidths $\Delta\omega_k$ are computed as

$$A_k = \sqrt{2S_{PM}(\omega_k)\Delta\omega_k} \quad (27)$$

Now an appropriate range of frequencies must be selected. Figure 3 shows that wave amplitude is near zero for frequencies less than one quarter the peak frequency and greater than 4 times the peak frequency. To obtain good resolution over this frequency range, one-third octave bands in the range $[\frac{\omega_0}{4}, 4\omega_0]$ are used. Band frequency limits and bandwidth are given in Table 2.

Figure 4 shows a wave for sea state 5 generated using this approach.

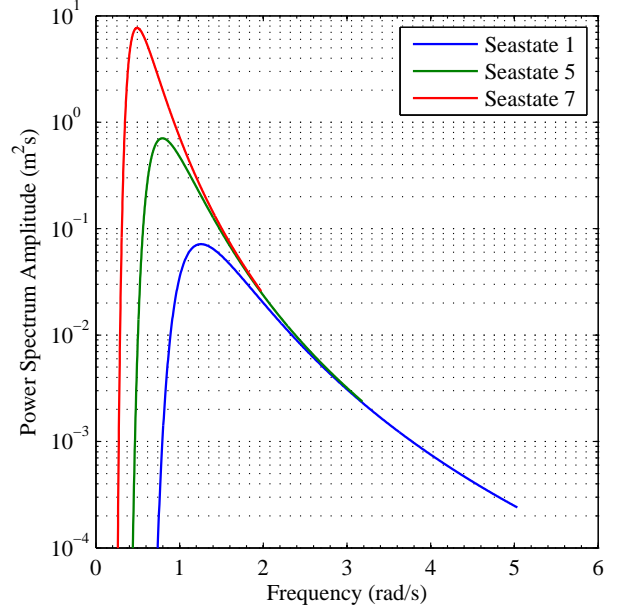


Fig. 3. Pierson-Moskowitz amplitude spectrum for Sea State 1, 5, and 7

Fast Ferry Ship Model Ship motion is wave motion modulated by ship dynamics. The two previous deck motion models do not include ship dynamics, thus a model of direct ship motion is useful to assess estimator performance.

In (Ref. 17) Hess defines a motion model for a TMV 114 fast ferry. This ship is 113.5m in length, has beam 16.5m and displacement 700 metric tonnes (Figure 5).

Table 2. One-third octave band frequencies in terms of ω_0

Center	Lower	Upper	Bandwidth
$0.25\omega_0$	$0.2227\omega_0$	$0.2806\omega_0$	$0.0579\omega_0$
$0.315\omega_0$	$0.2806\omega_0$	$0.3536\omega_0$	$0.0729\omega_0$
$0.397\omega_0$	$0.3536\omega_0$	$0.4455\omega_0$	$0.0919\omega_0$
$0.5\omega_0$	$0.4455\omega_0$	$0.5612\omega_0$	$0.1158\omega_0$
$0.63\omega_0$	$0.5612\omega_0$	$0.7071\omega_0$	$0.1459\omega_0$
$0.794\omega_0$	$0.7071\omega_0$	$0.8909\omega_0$	$0.1838\omega_0$
ω_0	$0.8909\omega_0$	$1.123\omega_0$	$0.2316\omega_0$
$1.26\omega_0$	$1.123\omega_0$	$1.414\omega_0$	$0.2918\omega_0$
$1.587\omega_0$	$1.414\omega_0$	$1.782\omega_0$	$0.3676\omega_0$
$2\omega_0$	$1.782\omega_0$	$2.245\omega_0$	$0.4631\omega_0$
$2.52\omega_0$	$2.245\omega_0$	$2.828\omega_0$	$0.5835\omega_0$
$3.175\omega_0$	$2.828\omega_0$	$3.564\omega_0$	$0.9263\omega_0$
$4\omega_0$	$3.564\omega_0$	$4.489\omega_0$	$1.167\omega_0$

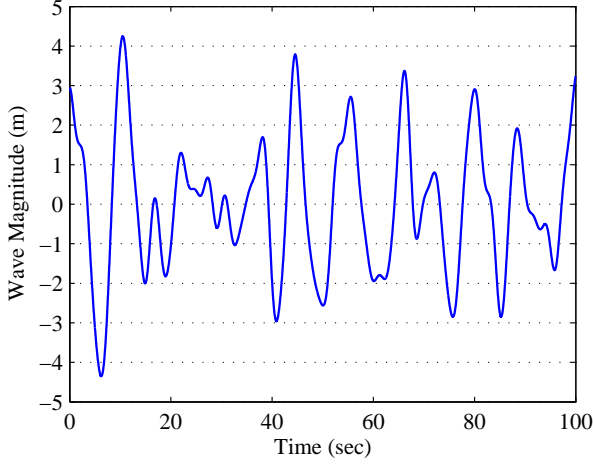


Fig. 4. Sample wave amplitude generated using 1/3 octave band Pierson-Moskowitz spectrum (sea state 5).



Fig. 5. TMV 114 fast ferry (Ref. 17).

Hess defines the EOMS for the ferry as:

$$y = 6.6 \sin \phi \quad (28)$$

$$z = 57.11 \sin \theta + 13.2 \sin^2 0.5\phi + 0.2172 \sin 0.4t + 0.4174 \sin 0.5t + 0.3592 \sin 0.6t + 0.2227 \sin 0.7t \quad (29)$$

$$\phi = 0.021 \sin 0.46t + 0.0431 \sin 0.54t + 0.290 \sin 0.62t + 0.022 \sin 0.67t \quad (30)$$

$$\theta = 0.005 \sin 0.46t + 0.00964 \sin 0.58t + 0.00725 \sin 0.7t + 0.00845 \sin 0.82t \quad (31)$$

The x position, and yaw angle are not as simply defined. For this research, x position and yaw angle wave forces were left to be determined by the stochastic model, while the other four wave forces use this ferry wave model.

ESTIMATOR DESIGN

Unscented Kalman Filter

The unscented Kalman Filter (UKF) is a non-linear Kalman filter that propagates an uncertain state through nonlinear equations using a discrete set of points (*sigma points*). The estimate mean and covariance are then recovered from the propagated sigma points. This approach is accurate to at least

second order: in contrast, and Extended Kalman Filter (EKF) is only accurate to first order (and has similar computational complexity). Details of the UKF can be found in (Ref. 18); an application to vision-based state estimation can be found in (Ref. 4).

The UKF follows the familiar recursive process of prediction (time update) followed by correction (vision update).

Time update The deck kinematics developed earlier can be written compactly as

$$\dot{\mathbf{x}}_d = f(\mathbf{x}_d) + \begin{bmatrix} \mathbf{0}_6 \\ \mathbf{I}_6 \end{bmatrix} \mathbf{F}_d \quad (32)$$

where $\mathbf{F}_d \sim \mathcal{N}(0, \mathbf{Q})$. In discrete form one can write

$$\mathbf{x}_{d,k+1} = f(\mathbf{x}_{d,k}) + \mathbf{v}_k \quad (33)$$

and one must determine the statistics of \mathbf{v}_k . To do so, consider the equations of deck motion for small angular displacements, which can be obtained from Equations 2.10 to 2.21 as

$$\dot{\mathbf{x}}_d = \begin{bmatrix} \mathbf{0}_6 & \mathbf{I}_6 \\ \mathbf{0}_6 & \mathbf{0}_6 \end{bmatrix} \mathbf{x}_d + \begin{bmatrix} \mathbf{0}_6 \\ \mathbf{I}_6 \end{bmatrix} \mathbf{F}_d \quad (34)$$

where $\mathbf{0}_6$ and \mathbf{I}_6 are 6×6 zero and identity matrices, respectively. Using a zero-order hold to discretize the equations of motion over a time step Δt gives

$$\mathbf{x}_{d,k+1} = \begin{bmatrix} \mathbf{I}_6 & \Delta t \mathbf{I}_6 \\ \mathbf{0}_6 & \mathbf{I}_6 \end{bmatrix} \mathbf{x}_{d,k} + \begin{bmatrix} \frac{\Delta t^2}{2} \mathbf{I}_6 \\ \Delta t \mathbf{I}_6 \end{bmatrix} \mathbf{F}_d \quad (35)$$

Thus $\mathbf{v}_k \sim \mathcal{N}(0, \bar{\mathbf{Q}})$ with

$$\bar{\mathbf{Q}} = \begin{bmatrix} \frac{\Delta t^2}{2} \mathbf{I}_6 \\ \Delta t \mathbf{I}_6 \end{bmatrix} \mathbf{Q} \begin{bmatrix} \frac{\Delta t^2}{2} \mathbf{I}_6 & \Delta t \mathbf{I}_6 \end{bmatrix} \quad (36)$$

Finally, it is assumed that \mathbf{Q} is diagonal (i.e. the process noise that models wave acceleration is uncorrelated in each of its components), so that

$$\mathbf{Q} = \begin{bmatrix} \sigma_u^2 & 0 & 0 & 0 & 0 & 0 \\ 0 & \sigma_v^2 & 0 & 0 & 0 & 0 \\ 0 & 0 & \sigma_w^2 & 0 & 0 & 0 \\ 0 & 0 & 0 & \sigma_p^2 & 0 & 0 \\ 0 & 0 & 0 & 0 & \sigma_q^2 & 0 \\ 0 & 0 & 0 & 0 & 0 & \sigma_r^2 \end{bmatrix} \quad (37)$$

Here $\sigma_{(\cdot)}$ represents the standard deviation of expected acceleration in that component. Recall that for sinusoidal deck motion

$$F_{d(\cdot)}(t) = -A_{(\cdot)} \omega_{(\cdot)}^2 \sin(\omega_{(\cdot)} t + \phi_{(\cdot)}) \quad (38)$$

and peak expected acceleration is thus $A_{(\cdot)} \omega_{(\cdot)}^2$. Both wave amplitude and frequency depend on sea state, and these may vary somewhat: Table 3 gives expected ranges for sea states 1, 5, and 7. Merely choosing the expected wave amplitude and frequency for a particular sea state and computing expected

acceleration will thus result in under-predicting wave excitation; choosing

$$\sigma_{(\cdot)} = \left(A_{(\cdot)}^{nom} + 3\sigma_A \right) \left(\omega_{(\cdot)}^{nom} + 3\sigma_\omega \right)^2 \quad (39)$$

will both ensure that a broad range of possible amplitudes and frequencies for a particular sea state is covered.

Vision update The vision update step is driven by the camera measurement model of Equation 20. It is assumed that the intrinsic camera parameters are known via calibration and that the remaining uncertainty in camera measurements can be adequately described by zero-mean Gaussian noise.

Data Association

Data association is a critical component of the deck state estimator. Failure to correctly associate measured bearings with the corresponding marker will almost certainly lead to divergence of the deck state estimator.

Data association is an example of an assignment problem. This class of problems has been extensively studied in the computer science literature and in robotics applications (especially problems related to simultaneous localization and mapping, or SLAM) (Refs. 19–21).

In this research, data association is computed by comparing the pixel location of a marker in the current image frame with pixel locations of markers in the previous frame. Close matches are assumed to come from the same marker. In this case “close” is computed as the Mahalanobis Distance:

$$d_{nm} = (z_n - z_m)^T P_{mm}^{-1} (z_n - z_m) \quad (40)$$

Here z_m is the expected pixel location of a marker from the previous frame in the current frame and z_n is the measured pixel location of a marker in the current frame. The matrix P_{mm} represents the uncertainty of the expected marker position. The quantity d_{nm} thus represents the distance (scaled by uncertainty) between a measured marker location and the expected marker location.

This distance is computed for all possible combinations, leading to an $n \times m$ distance matrix:

$$D = \begin{bmatrix} d_{11} & d_{12} & \cdots & d_{1m} \\ d_{21} & d_{22} & \cdots & d_{2m} \\ \vdots & & & \vdots \\ d_{n1} & \cdots & \cdots & d_{nm} \end{bmatrix} \quad (41)$$

The problem now is to compute the assignments that minimize the overall cost. One approach is to begin with the top row and assign the markers in turn based on minimum distance. This “greedy” approach is brittle, however, and may lead to incorrect assignment in cases of ambiguity (i.e. similar distances for several possible assignments).

A better approach is to minimize the total cost. In large assignment problems (with tens or hundreds of markers) it

can quickly become computationally prohibitive to brute force this problem (i.e. compute cost of all possible assignments, choose the lowest net cost). Here the Munkres Algorithm (Ref. 22) is used to compute the minimum-cost data association.

Deck Estimate Initialization

It is assumed that a single message giving ship speed and heading and sea state is transmitted to the helicopter at the beginning of the approach to the deck. Since no information about deck height, roll, or pitch is given these states are initialized to zero with some associated covariance, so that

$$\hat{\mathbf{x}}_{d,0} = [0 \ 0 \ 0 \ 0 \ 0 \ \psi_0 \ u_0 \ v_0 \ 0 \ 0 \ 0 \ 0]^T \quad (42)$$

The initial covariance is assumed to be diagonal, with magnitudes of the individual components dependent on sea state. For each component of the state the standard deviation is set to the root mean square value of the expected amplitude of motion, so that

$$\mathbf{P}_0(\cdot) = \frac{1}{2} A_{(\cdot)}^2 \quad (43)$$

for $x, y, z, \phi, \theta, \psi$ and

$$\mathbf{P}_0(\cdot) = \frac{1}{2} A_{(\cdot)}^2 \omega_{(\cdot)}^2 \quad (44)$$

for u, v, w, p, q, r . Expected amplitudes and frequencies for sea states 1, 5, and 7 are given in Table 3. Data in Table 3 were computed from (Ref. 23).

SIMULATION RESULTS

Monte Carlo simulations are used to assess performance of the deck state estimator. Each Monte Carlo simulation consists of fifty runs with random seas generated for each run. Results for both the stochastic wave model and the fast ferry model are presented: for the stochastic model sea states 1, 5 and 7 are examined. The fast ferry model from (Ref. 17) is for moderate seas (sea state 4).

The ship is traveling at a nominal speed of 3 m/s (5.8 kts). The helicopter begins from a point 250 meters behind and 100 meters above the ship, and it travels at a constant speed of 14.5 m/s (28 kts) in a straight line towards the ship deck. The simulation starts at time zero and ends at $t = 20$ seconds, when the helicopter is approximately 15 meters behind and 8 meters above the ship deck.

Helicopter Kinematics

Since the focus here is on estimation (and not flight control or path planning) a kinematic model is used for the helicopter. The state vector is given in Equation 2 and control inputs are

$$\mathbf{u}_h = [p_h \ q_h \ r_h \ T_x \ T_y \ T_z]^T \quad (45)$$

It is thus implicitly assumed that an on-board flight controller can follow angular rate commands and can compute

Table 3. Wave data for sea states 1, 5, 7

component	mean Amp.	Amp. Variance	mean Period	Period Variance
Seastate 1				
x	0.2 m	0.1 m ²	5 sec	1 sec ²
y	0.2 m	0.1 m ²	5 sec	1 sec ²
z	0.5 m	0.2 m ²	5 sec	1 sec ²
ϕ	4°	2° ²	5 sec	1 sec ²
θ	1°	1° ²	5 sec	1 sec ²
ψ	1°	1° ²	5 sec	1 sec ²
Seastate 5				
x	1 m	0.5 m ²	12 sec	3 sec ²
y	1 m	0.5 m ²	12 sec	3 sec ²
z	2.5 m	1 m ²	12 sec	3 sec ²
ϕ	12°	3° ²	12 sec	3 sec ²
θ	5°	2° ²	12 sec	3 sec ²
ψ	3°	1° ²	12 sec	3 sec ²
Seastate 7				
x	2.6 m	1.3 m ²	17 sec	4 sec ²
y	2.6 m	1.3 m ²	17 sec	4 sec ²
z	6.5 m	2.5 m ²	17 sec	4 sec ²
ϕ	35°	9° ²	17 sec	4 sec ²
θ	12°	3° ²	17 sec	4 sec ²
ψ	4°	3° ²	17 sec	4 sec ²

(within constraints) the desired magnitude and direction of the net thrust vector. Equations of motion for small angles are

$$\dot{x}_h = u(\cos \psi_h) - v_h(\sin \psi_h) \quad (46)$$

$$+ w_h(\theta_h \cos \psi_h + \phi_h \sin \psi_h)$$

$$\dot{y}_h = u_h(\sin \psi_h) - v_h(\cos \psi_h) \quad (47)$$

$$+ w_h(\theta_h \sin \psi_h - \phi_h \cos \psi_h)$$

$$\dot{z}_h = (-\theta_h)u_h + (\phi_h)v_h + w_h \quad (48)$$

$$\dot{\phi}_h = p_h - (\theta_h)r_h \quad (49)$$

$$\dot{\theta}_h = q_h - (\phi_h)r_h \quad (50)$$

$$\dot{\psi}_h = (\phi_h)q_h - r_h \quad (51)$$

$$\dot{u}_h = -(w_h q_h - v_h r_h) + T_x/m - g \theta_h \quad (52)$$

$$\dot{v}_h = -(u_h r_h - w_h p_h) + T_y/m + g \phi_h \quad (53)$$

$$\dot{w}_h = -(v_h p_h - u_h q_h) + T_z/m + g \quad (54)$$

For constant speed flight along a specified flight path angle (a steady state condition) the required control inputs can be computed. Similarly, control inputs to follow a desired flight path (for example, to maximize information gained about the landing deck during approach) can also be computed.

Sea state conditions

For each run a new random sea condition was generated using the statistics of Table 3 for amplitude and frequency and a random set of phases. The sum-of-sinusoids of Equation 24 was then used to generate the sea conditions.

UKF parameters

Filter process noise is computed using Equations (36, 37, 39). Camera measurement noise has standard deviation 1°.

Helicopter state is assumed to be known with precision. In practice, knowledge of angles will be limited to a standard deviation of 1° to 2°, but this uncertainty can be included in the camera bearing measurement uncertainty. Noise in the helicopter position estimate will have a much smaller effect than angular uncertainty.

Pierson-Moskowitz Wave Model Results

Results of a representative run of deck state estimation for sea state 5 are shown in Figure 6 and Figure 7. Plots show true deck state, estimated deck state and 2σ bounds. True states are generally within ±σ of estimated states, indicating a generally consistent estimate. The errors in state estimates become progressively smaller as the helicopter approaches the deck: this occurs because deck state is continuously updated as measurements are received and because the effect of noise in bearing measurements on computed deck state is smaller at short range. By the end of the simulation (when the helicopter is close to the deck): the error in deck position estimate is 0.43 meters; the error in deck orientation estimate is 0.5 degrees; the error in deck velocity estimate is 0.4 m/s; and the error in deck angular rate is 5.6 degrees per second.

Results of Monte Carlo simulations for sea states 1, 5, and 7 are given in Figure 8 through Figure 12. The true error

(shown in grey and as a blue line) remains bounded throughout the simulation and gets smaller as the deck is approached. The mean estimated variance (shown as a red dashed line) is somewhat smaller than the mean true variance, indicating that the estimator is slightly over-confident in its computation of states. However, errors (especially deck position error) is small.

Sea state affects both true error variance and the estimated error variance, with higher sea states resulting in higher variance. This is to be expected: at higher sea states the disturbance acting on the deck is significantly greater than at lower sea states.

Examining components of the estimator variance shows that the greatest contributor to total error is in the velocity and angular rate states. Note that there is no measurement of deck velocity, which leads to this larger error. The availability of a deck velocity measurement (for example, via optical flow or tau-dot) should improve this considerably.

Fast Ferry Ship Model Results

Results of a representative run of deck state estimation using the fast ferry model are shown in Figure 13 and Figure 14. Again plots show true deck state, estimated deck state and 2σ bounds. As with the Pierson-Moskowitz model, the estimator tracks true states very well, with errors generally well within 2σ bounds. By the end of the simulation (when the helicopter is close to the deck): the error in deck position estimate is 0.24 meters; the error in deck orientation estimate is 0.7 degrees; the error in deck velocity estimate is 0.2 m/s; and the error in deck angular rate is 2.4 degrees per second.

Results of Monte Carlo simulations are given in Figure 15. Results are qualitatively similar to the sea state 5 results of the Pierson-Moskowitz model, with errors bounded and becoming smaller as the helicopter approaches the deck.

CONCLUSION

This paper has described a vision-based deck state estimation system applicable to the problem of autonomous (or aided) landing of a rotorcraft on a ship deck in moderate to rough seas. All sensing is carried on board the helicopter, and only a single message containing ship nominal heading and speed and sea state is sent to the helicopter at the beginning of the approach phase. The estimator assumes a second order kinematic model for the deck, with the intention of applicability across a wide variety of ships and boats.

Results of Monte Carlo simulations using a Pierson-Moskowitz wave model in sea states 1, 5, and 7 show that the estimator is able to produce generally consistent estimates of deck state (i.e. computed variance is a reasonable prediction of true error variance). The estimator is somewhat over-confident in its estimates (the computed variance is slightly lower than the true variance): some tuning of estimator parameters should improve this.

Monte Carlo simulations using a fast ferry ship model in moderate seas (approximately sea state 4) are also presented. Results are similar to those obtained using the Pierson-Moskowitz spectrum for ship deck motion.

The use of a second order kinematic model results in significant unmodeled dynamics, but there is significant advantage in the generality of the resulting estimator to variations of both sea state and deck motion dynamics.

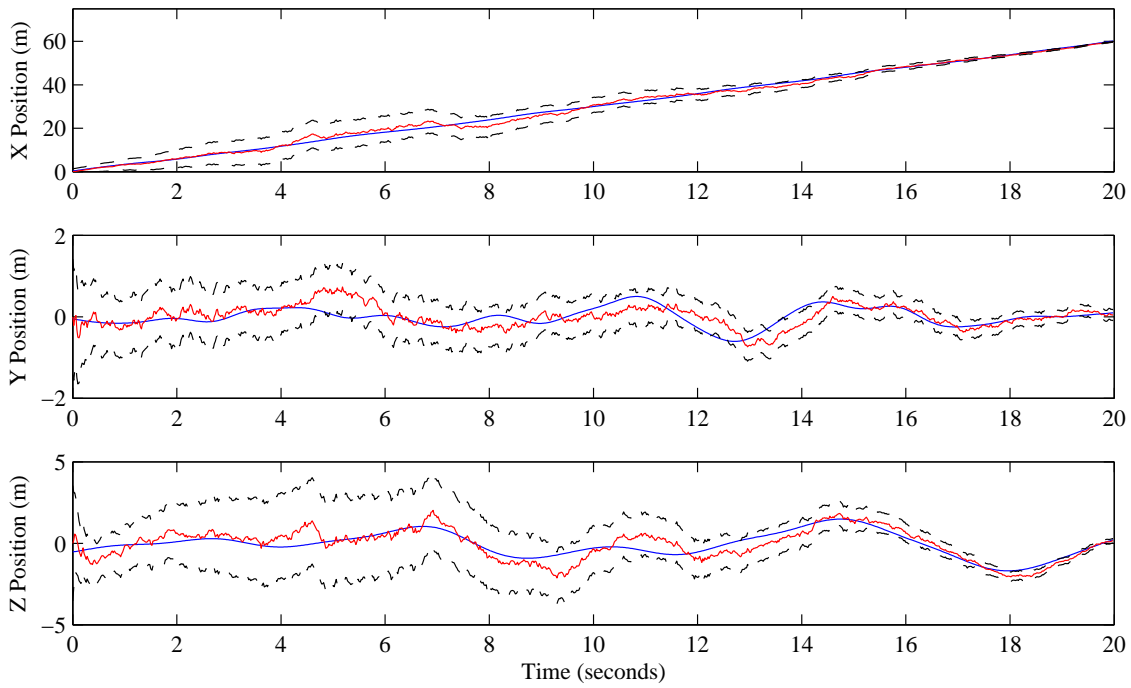
ACKNOWLEDGMENTS

This research is partially funded by the Government under Agreement No. W911W6-11-2-0011. The U.S. Government is authorized to reproduce and distribute reprints notwithstanding any copyright notation thereon. The views and conclusions contained in this document are those of the authors and should not be interpreted as representing the official policies, either expressed or implied, of the U.S. Government.

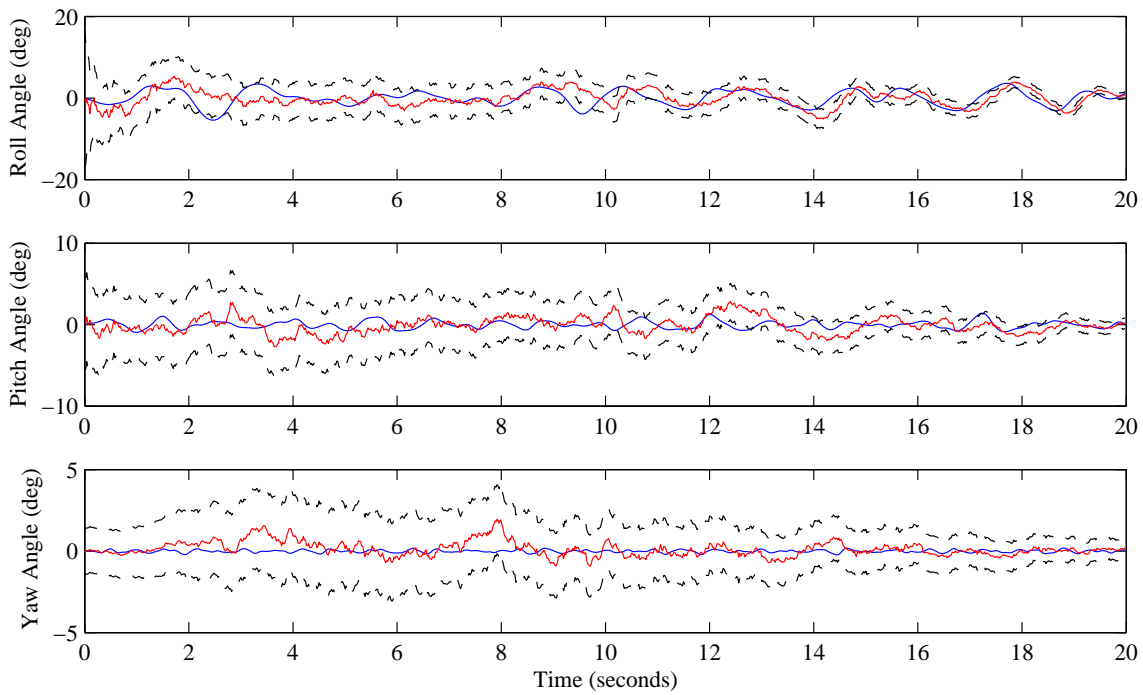
REFERENCES

- ¹Bernard de Ferrier, P. and Manning, T., "Simulation and Testing of the Landing Period Designator (LPD) Helicopter Recovery Aid," *Naval Engineers Journal*, Vol. 110, (1), January 1998, pp. 189–205.
- ²Oh, S.-R., Pathak, K., Agrawal, S. K., Pota, H. R., and Garratt, M., "Approaches for a Tether-Guided Landing of an Autonomous Helicopter," *IEEE Transactions on Robotics*, Vol. 22, (3), June 2006, pp. 189–205.
- ³Sinopoli, B., Micheli, M., Donato, G., and Koo, T. J., "Vision Based Navigation for an Unmanned Aerial Vehicle," Proceedings of the IEEE International Conference on Robotics and Automation (ICRA), May 2001.
- ⁴Langelan, J. W., "State Estimation for Autonomous Flight in Cluttered Environments," *Journal of Guidance, Control and Dynamics*, Vol. 30, (5), September-October 2007, pp. 1414–1426.
- ⁵Diel, D. D., DeBitetto, P., and Teller, S., "Epipolar Constraints for Vision-Aided Inertial Navigation," IEEE Workshop on Motion and Video Computing, 2005.
- ⁶Wu, A. D., Johnson, E. N., and Proctor, A. A., "Vision-Aided Inertial Navigation for Flight Control," AIAA Guidance, Navigation and Control Conference, August 2005.
- ⁷Webb, T. P., Prazenica, R. J., Kurdila, A. J., and Lind, R., "Vision-Based State Estimation for Autonomous Micro Air Vehicles," *Journal of Guidance, Control and Dynamics*, Vol. 30, (3), May-June 2007, pp. 816–827.
- ⁸Proctor, A. and Johnson, E. N., "Vision-only Approach and Landing," AIAA Guidance, Navigation and Control Conference, August 2005.

- ⁹Johnson, E. N., Calise, A. J., Watanabe, Y., Ha, J., and Neidhoefer, J. C., “Real-Time Vision-Based Relative Navigation,” AIAA Guidance, Navigation and Control Conference and Exhibit, August 21-24 2006.
- ¹⁰Millet, P. T., Ready, B. B., and McLain, T. W., “Vision-Based Precision Landings of a Tailsitter UAV,” AIAA Guidance, Navigation and Control Conference, August 10-13 2009.
- ¹¹Saripalli, S., Montgomery, J. F., and Sukhatme, G. S., “Vision-based Autonomous Landing of an Unmanned Aerial Vehicle,” International Conference on Robotics and Automation, May 2002.
- ¹²Saripalli, S. and Sukhatme, G. S., “Landing a Helicopter on a Moving Target,” IEEE International Conference on Robotics and Automation, 2007.
- ¹³Saripalli, S., “Vision-based Autonomous Landing of an Helicopter on a Moving Target,” AIAA Guidance, Navigation and Control Conference, August 2009.
- ¹⁴Garratt, M., Pota, H., Lambert, A., Eckersley-Maslin, S., and Farabet, C., “Visual Tracking and LIDAR Relative Positioning for Automated Launch and Recovery of an Unmanned Rotorcraft from Ships at Sea,” *Naval Engineers Journal*, Vol. 121, (2), June 2009, pp. 99–110.
- ¹⁵Pérez, T. and Blanke, M., “Simulation of Ship Motion in Seaway,” Technical report ee02037, The University of Newcastle, Australia and Technical University of Denmark, 2002.
- ¹⁶Williard J. Pierson, J. and Moskowitz, L., “A Proposed Spectral Form for Fully Developed Wind Seas Based on the Similarity Theory of S. A. Kitaigorodskii,” *Journal of Geophysical Research*, Vol. 69, (24), December 1964, pp. 5181–5190.
- ¹⁷Hess, R. A., “Simplified Technique for Modeling Piloted Rotorcraft Operations Near Ships,” *Journal of Guidance, Control and Dynamics*, Vol. 29, (6), November-December 2006, pp. 1339–1349.
- ¹⁸van der Merwe, R. and Wan, E. A., “The square-root unscented Kalman filter for state and parameter-estimation,” IEEE International Conference on Acoustics, Speech, and Signal Processing, May 7-11 2001.
- ¹⁹Neira, J. and Tardós, J. D., “Data Association in Stochastic Mapping Using the Joint Compatibility Test,” *IEEE Transactions on Robotics and Automation*, Vol. 17, (6), December 2001, pp. 890–897.
- ²⁰Nieto, J., Guivant, J., Nebot, E., and Thrun, S., “Real Time Data Association for FastSLAM,” IEEE International Conference on Robotics and Automation (ICRA), 2003.
- ²¹Fitzgibbons, T. and Nebot, E., “Bearing Only SLAM using Colour-based Feature Tracking,” 2002 Australasian Conference on Robotics and Automation, 2002.
- ²²Kuhn, H. W., “The Hungarian Method for the Assignment Problem,” *Naval Research Logistics Quarterly*, 1955.
- ²³“Pierson-Moskowitz Sea Spectrum,” <http://www.sqwestinc.com/support/Sea%20State%20Table.htm>, last accessed April 15, 2013.

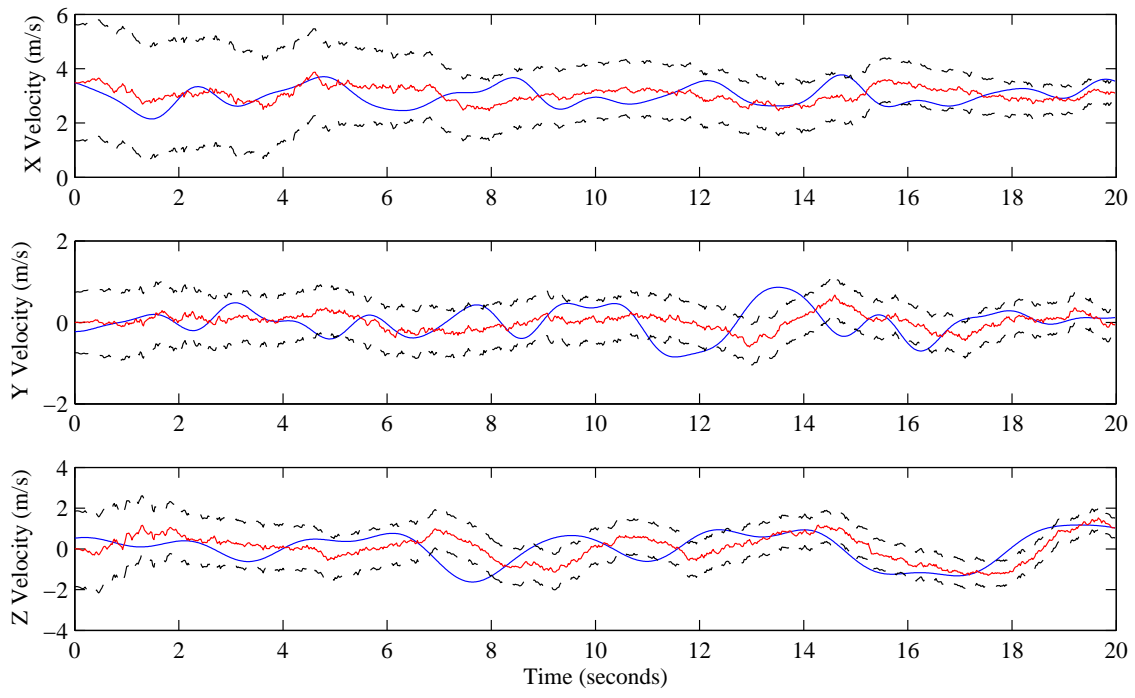


(a) Position estimation

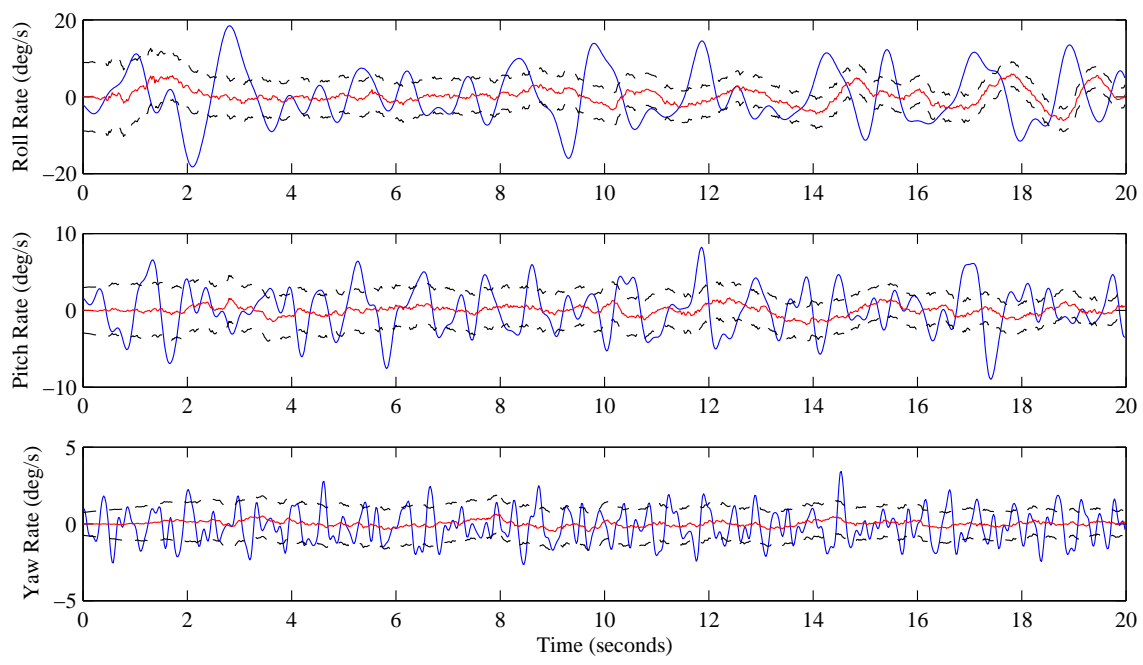


(b) Orientation estimation

Fig. 6. Representative run position and orientation estimation for Pierson-Moskowitz wave model. True state shown in blue, estimate shown in red, $\pm 2\sigma$ bounds shown as dashed lines.

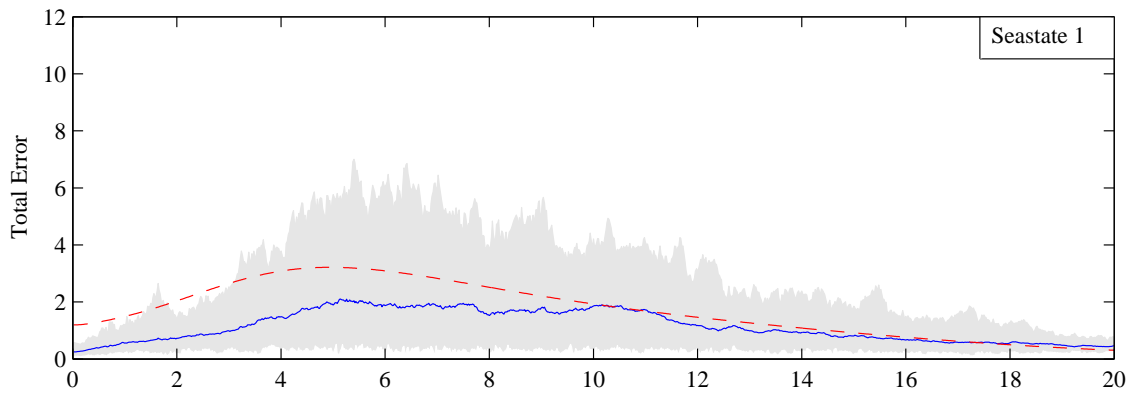


(a) Velocity estimation

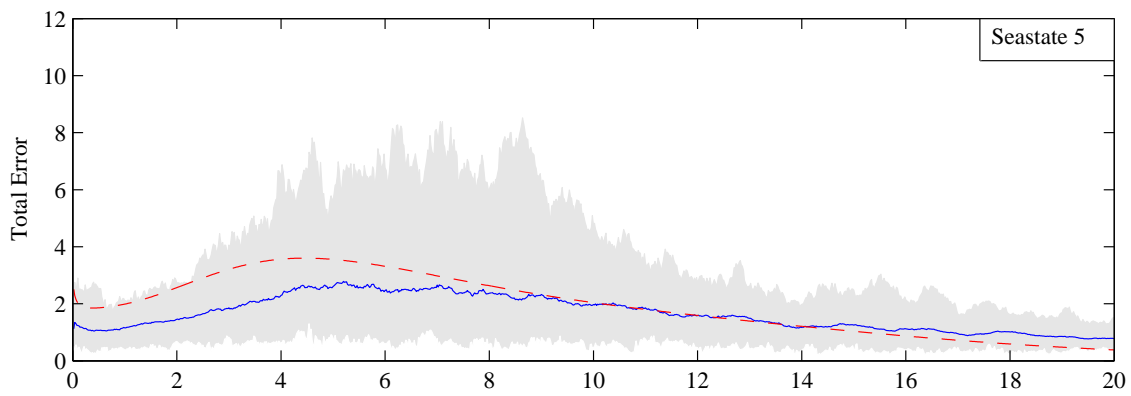


(b) angular rate estimation

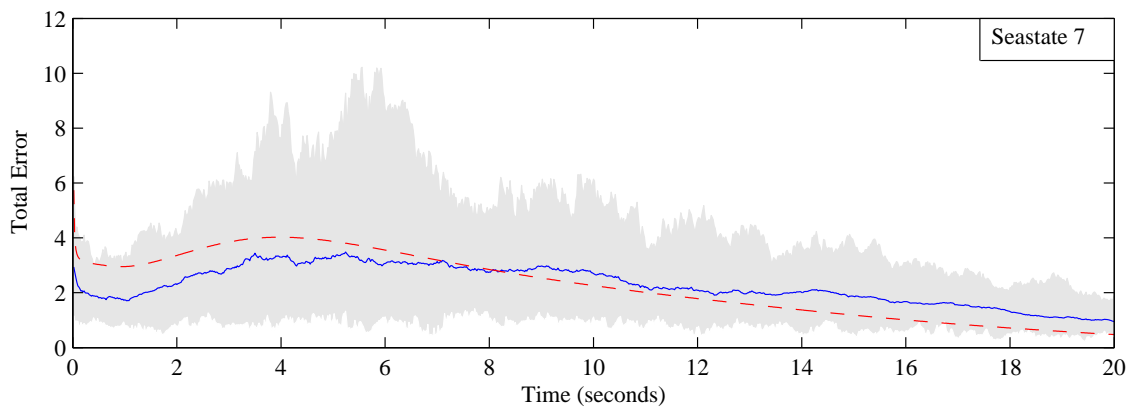
Fig. 7. Representative run velocity and angular rate estimation for Pierson-Moskowitz wave model. True state shown in blue, estimate shown in red, $\pm 2\sigma$ bounds shown as dashed lines.)



(a)

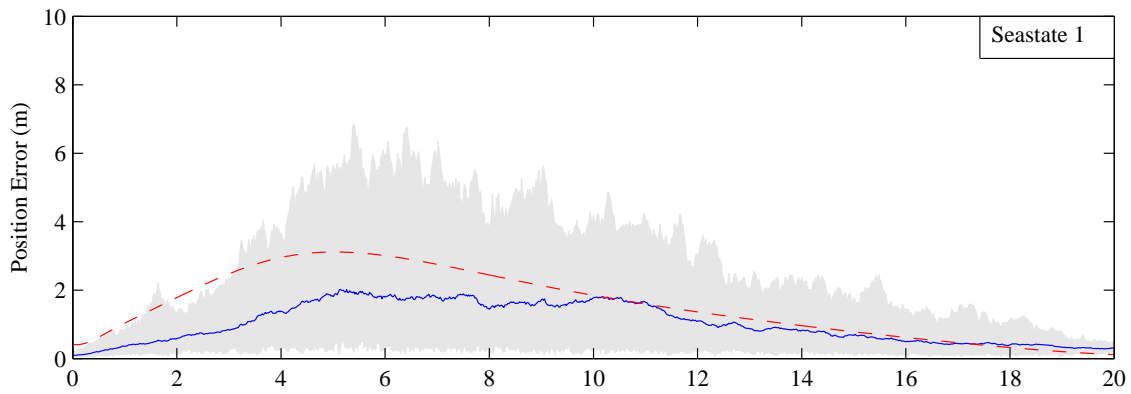


(b)

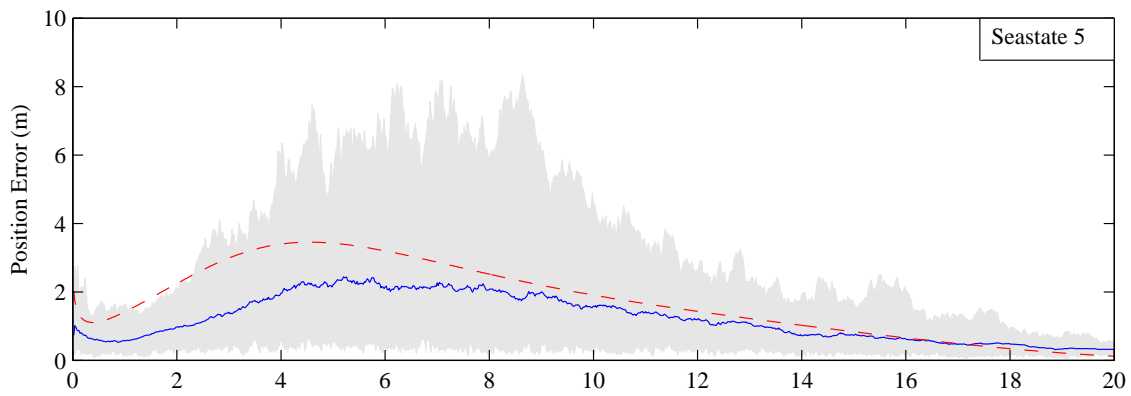


(c)

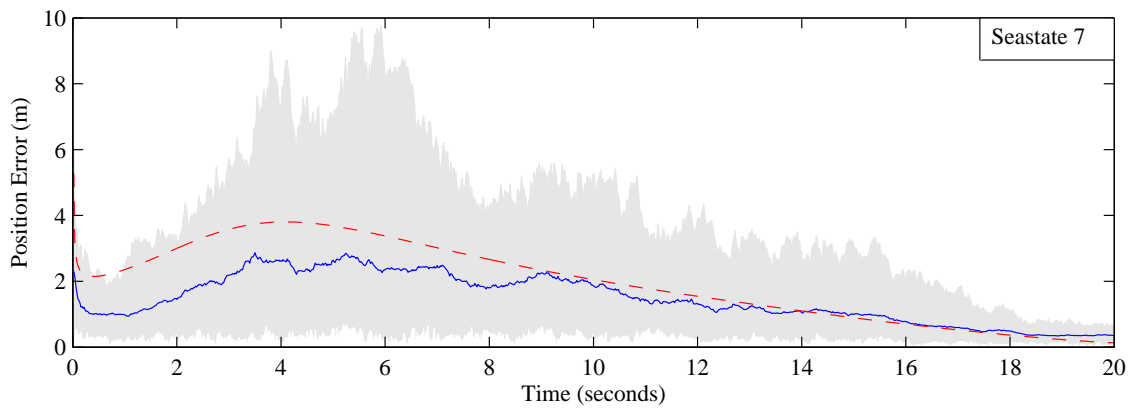
Fig. 8. Estimator total error for Pierson-Moskowitz waves for sea states 1, 5, 7 (from 50 run Monte Carlo simulation). The grey region shows max/min bounds of true error, blue line shows mean true error, red dashed line shows estimated total variance (i.e. $\sqrt{\text{TrP}}$).



(a)

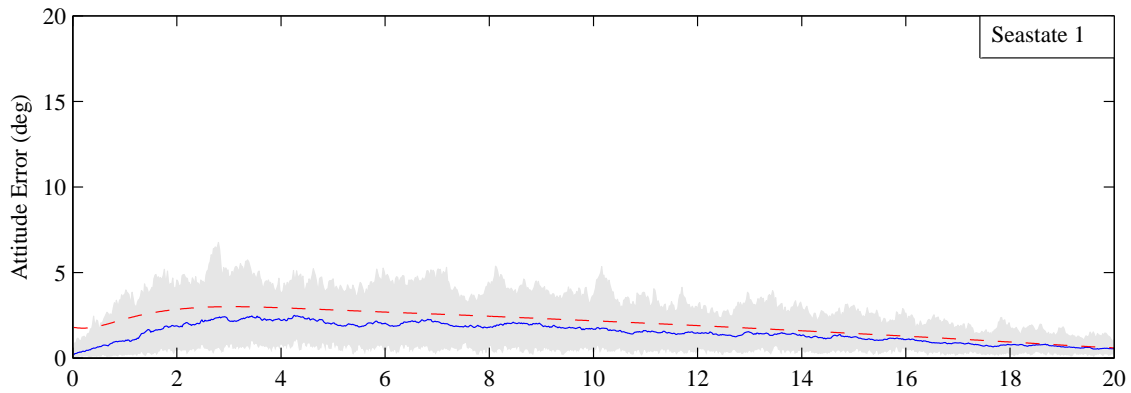


(b)

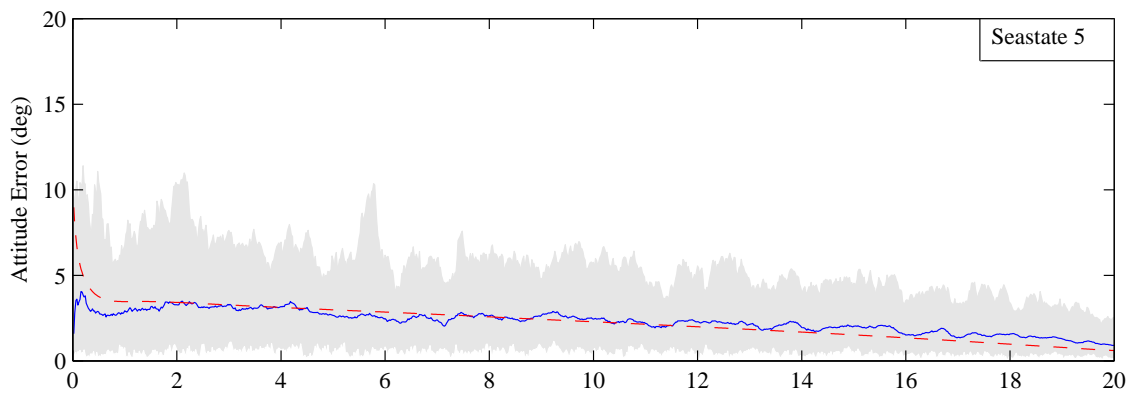


(c)

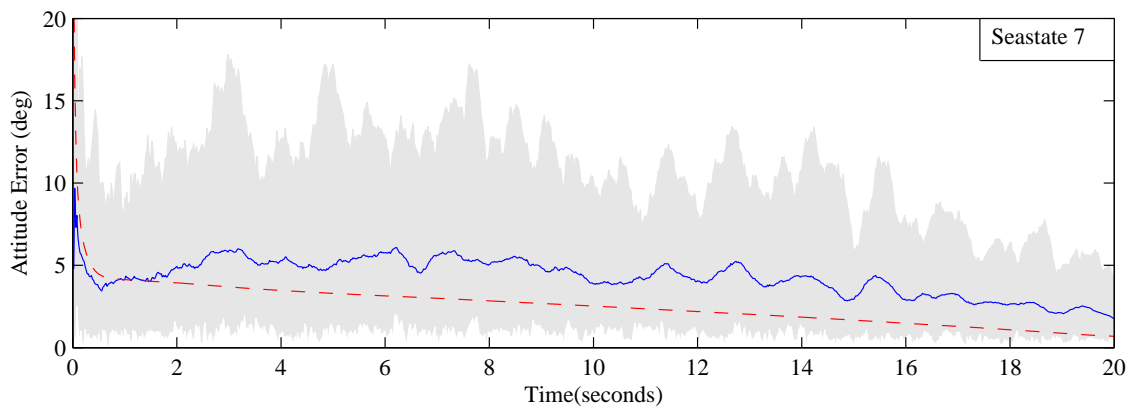
Fig. 9. Estimator position error for Pierson-Moskowitz waves for sea states 1, 5, 7 (from 50 run Monte Carlo simulation). The grey region shows max/min bounds of true error, blue line shows mean true error, red dashed line shows estimated variance in position estimates.



(a)

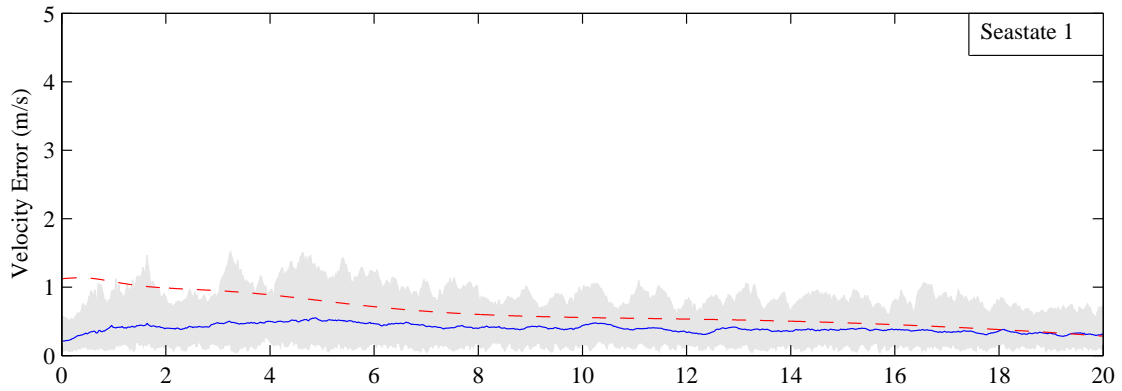


(b)

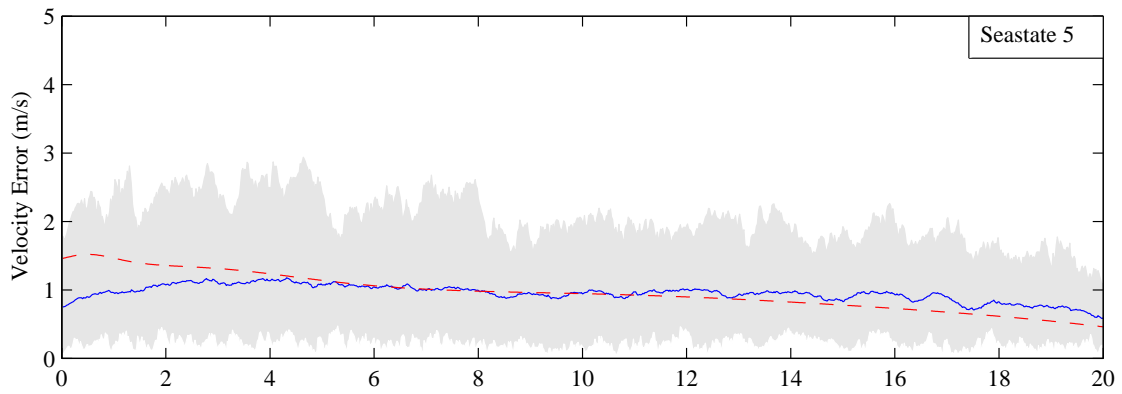


(c)

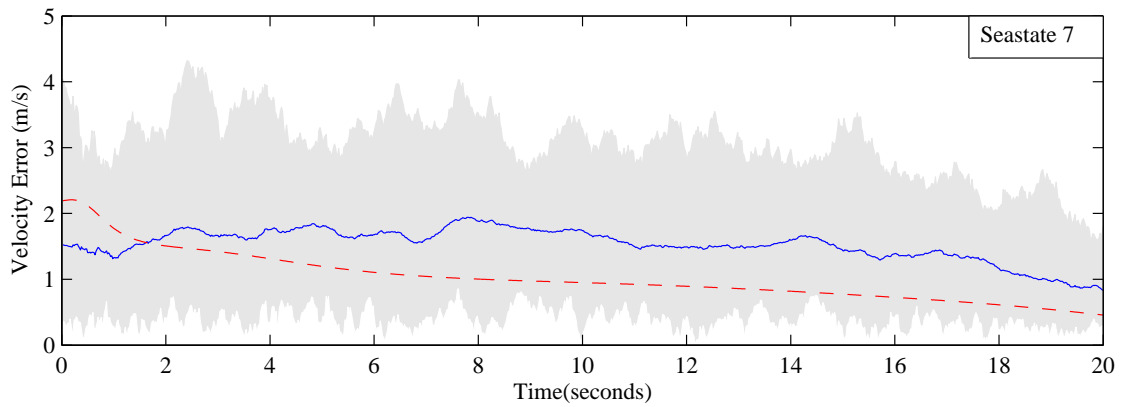
Fig. 10. Estimator orientation error for Pierson-Moskowitz waves for sea states 1, 5, 7 (from 50 run Monte Carlo simulation). The grey region shows max/min bounds of true error, blue line shows mean true error, red dashed line shows estimated variance in orientation estimates.



(a)

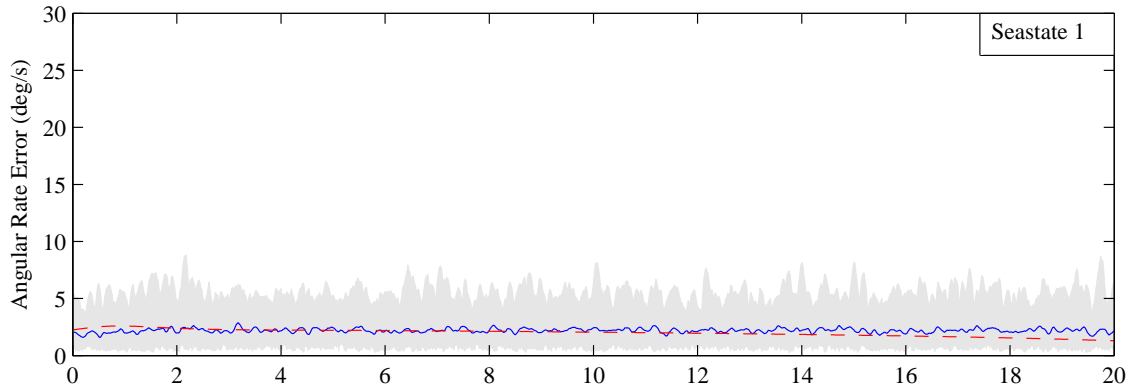


(b)

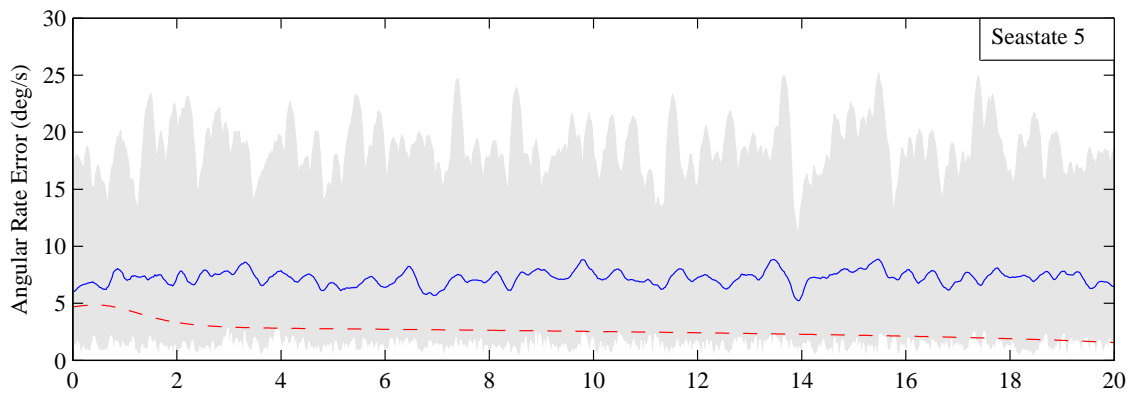


(c)

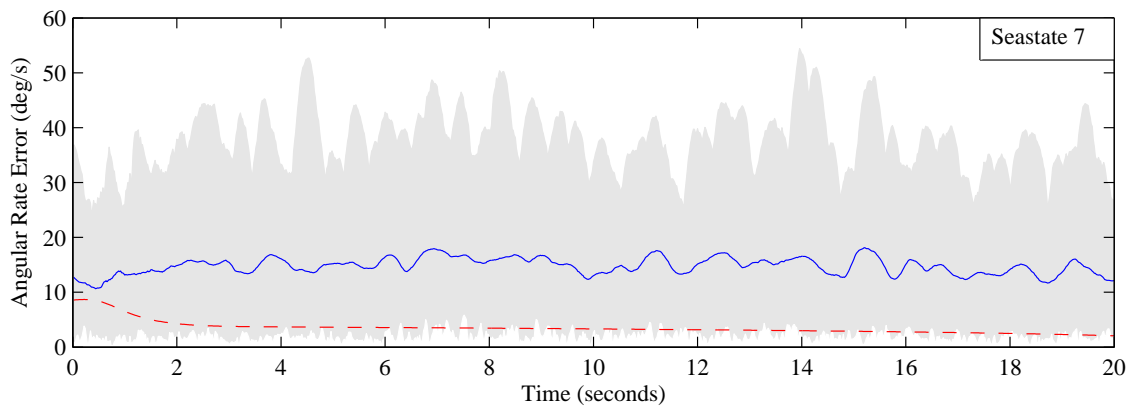
Fig. 11. Estimator velocity error for Pierson-Moskowitz waves for sea states 1, 5, 7 (from 50 run Monte Carlo simulation). The grey region shows max/min bounds of true error, blue line shows mean true error, red dashed line shows estimated variance in velocity estimates.



(a)

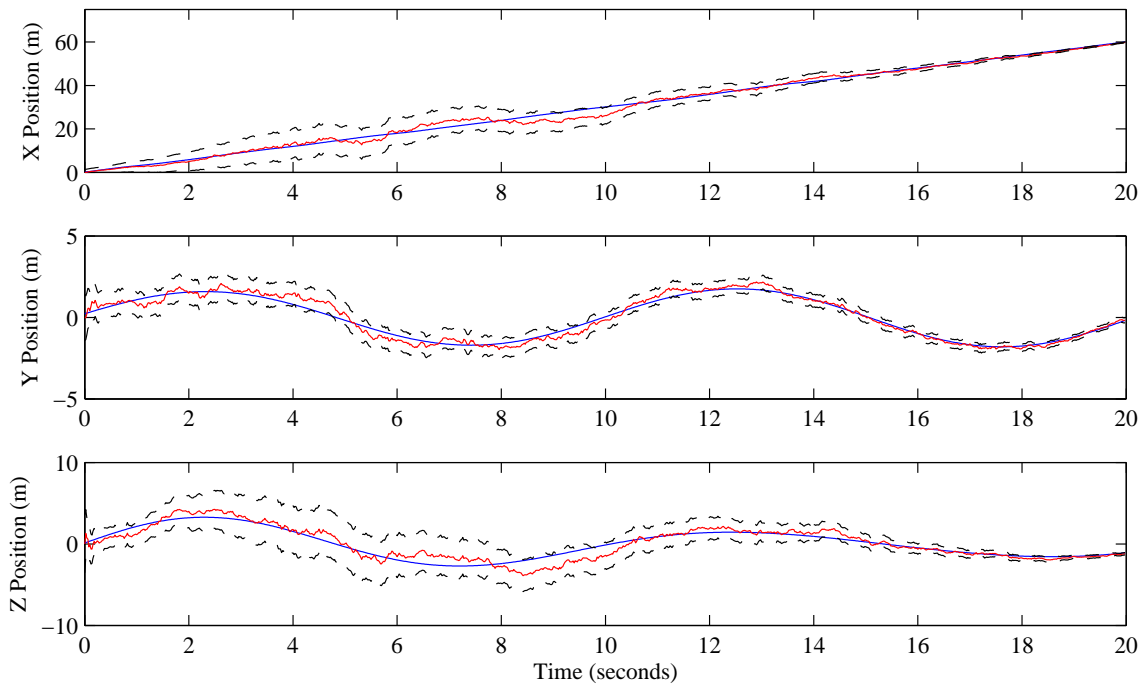


(b)

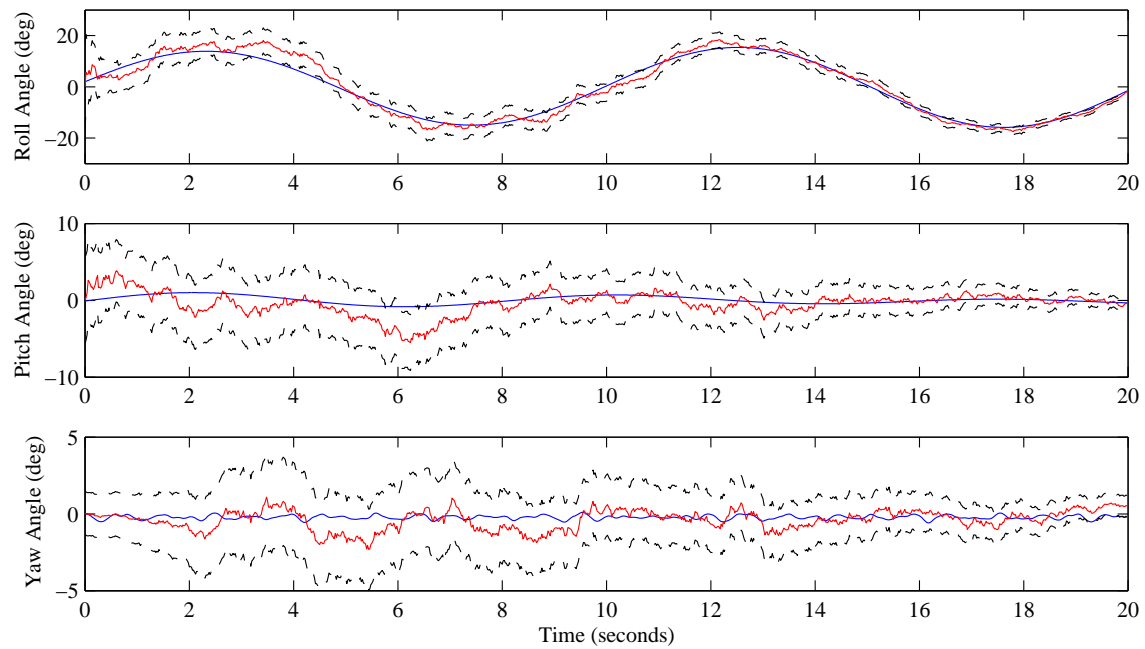


(c)

Fig. 12. Estimator angular rate error for Pierson-Moskowitz waves for sea states 1, 5, 7 (from 50 run Monte Carlo simulation). The grey region shows max/min bounds of true error, blue line shows mean true error, red dashed line shows estimated variance in angular rate estimates.

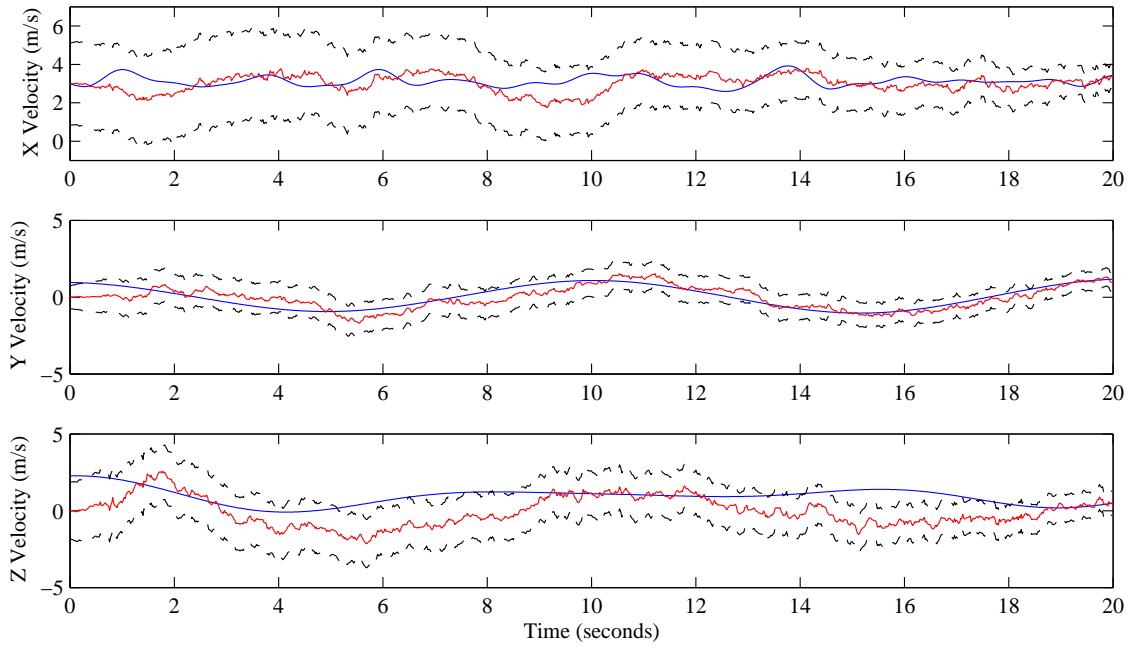


(a)

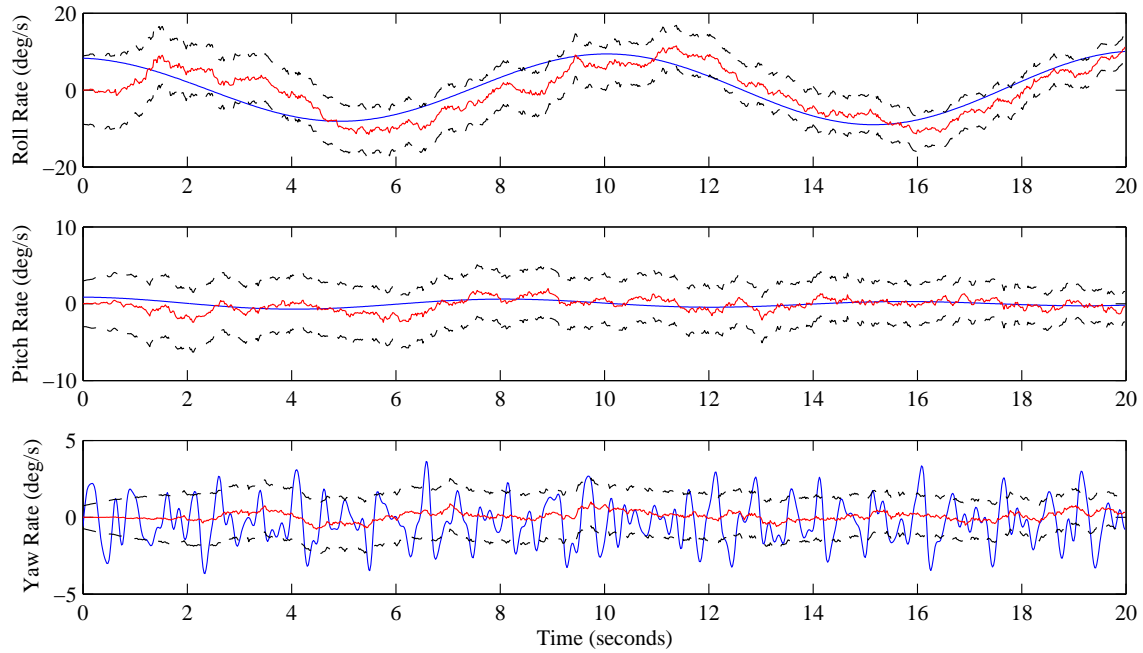


(b)

Fig. 13. Representative run position and orientation estimation for fast ferry ship model. True state shown in blue, estimate shown in red, $\pm 2\sigma$ bounds shown as dashed lines.



(a)



(b)

Fig. 14. Representative run velocity and angular rate estimation for fast ferry ship model. True state shown in blue, estimate shown in red, $\pm 2\sigma$ bounds shown as dashed lines.

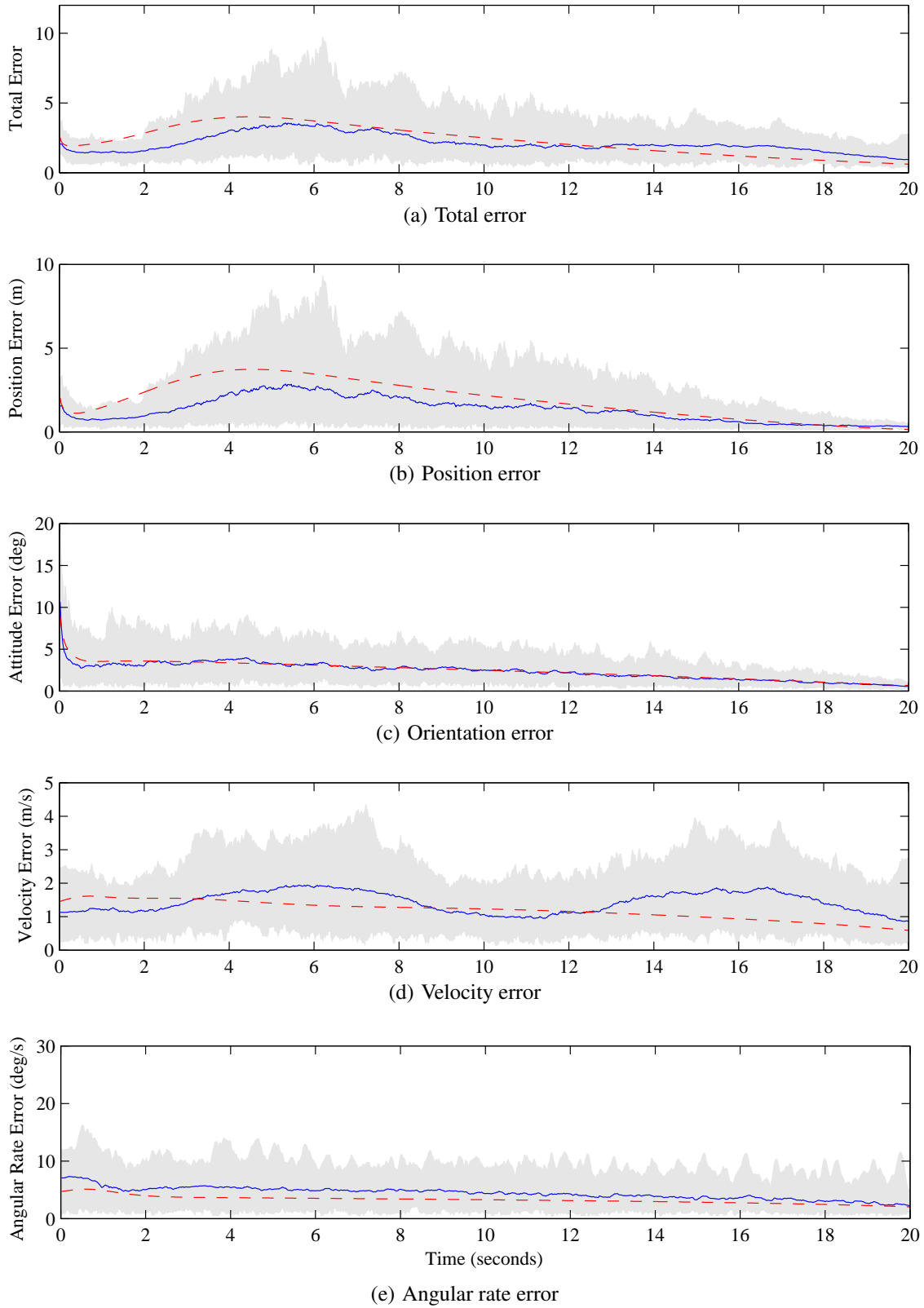


Fig. 15. Estimator error for fast ferry model (from 50 run Monte Carlo simulation). The grey region shows max/min bounds of true error, blue line shows mean true error, red dashed line shows estimated variance estimates.